Supporting Information for

Molecular Mechanisms of T221 Phosphorylation in Modulating SIK3 Kinase Function and ATP Binding

Shuo Wang[1,2], Yaoyue Zhang[1,2], Yujie Zhang[1,2], Zhihui Wang[1,2], Xiaoning Yao[1,2], Lidong Gong[1*], Guohui Li[1,2,3*], Anhui Wang[1,2,3*]

1. School of Chemistry and Chemical Engineering, Liaoning Normal University, Dalian, 116029, China.

2. Interdisciplinary Research Center for Biology and Chemistry, Liaoning Normal University, Dalian, 116029, China.

3. Laboratory of Molecular Modeling and Design, State Key Laboratory of Molecular Reaction Dynamics, Dalian Institute of Chemical Physics, Chinese Academy of Sciences, Dalian, 116023, China.

*Email: wangah@lnnu.edu.cn, ghli@dicp.ac.cn, gongjw@lnnu.edu.cn

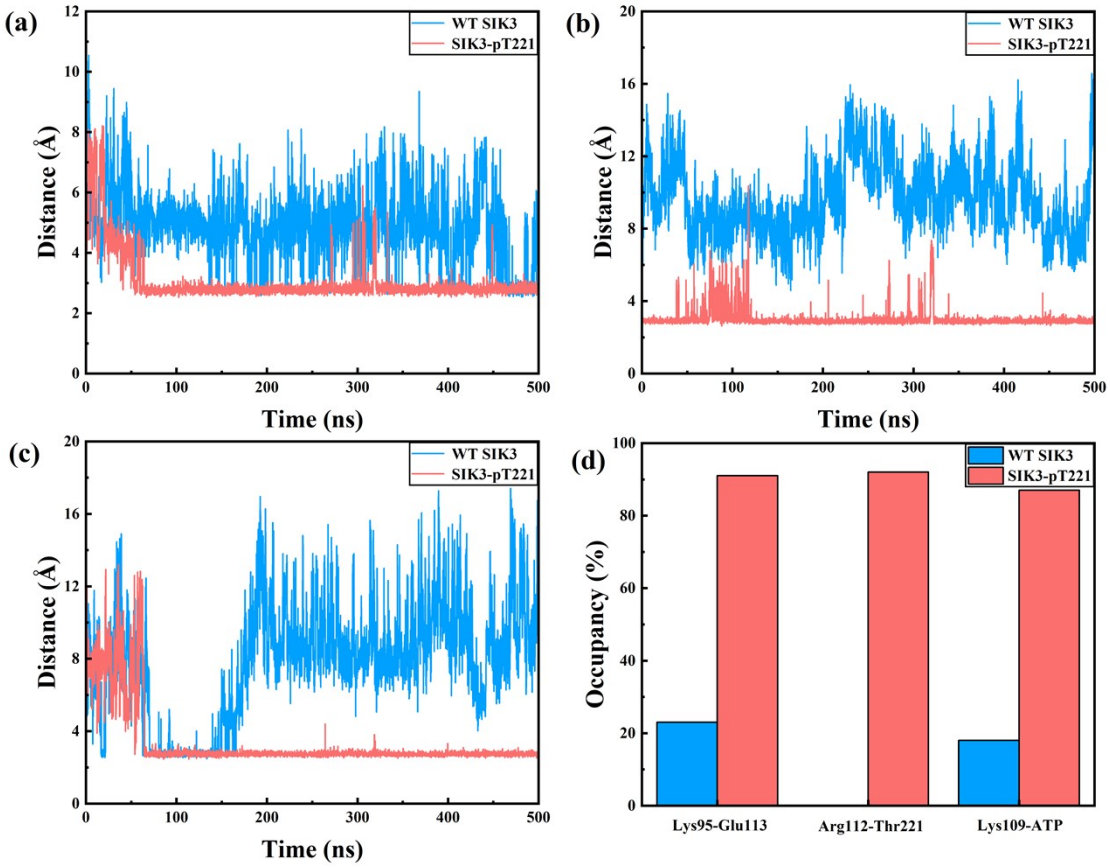

Figure S1. Effects of T221 phosphorylation on inter-residue distances and salt-bridge occupancies during MD simulations. (a) Time evolution of the minimum distance between Glu113 and Lys95. (b) Distance between Arg112 and the T221/pT221 side chain, showing formation of the Arg112–pT221 salt bridge upon phosphorylation. (c) Time-dependent distance between Lys109 and the phosphate group of ATP. (d) Overall occupancies of three key salt bridges (Glu113–Lys95, Arg112–pT221, and Lys109–ATP) throughout the simulations, comparing the WT SIK3 and the SIK3-pT221 systems. The WT SIK3 system is shown in blue, and the SIK3-pT221 system in light red.

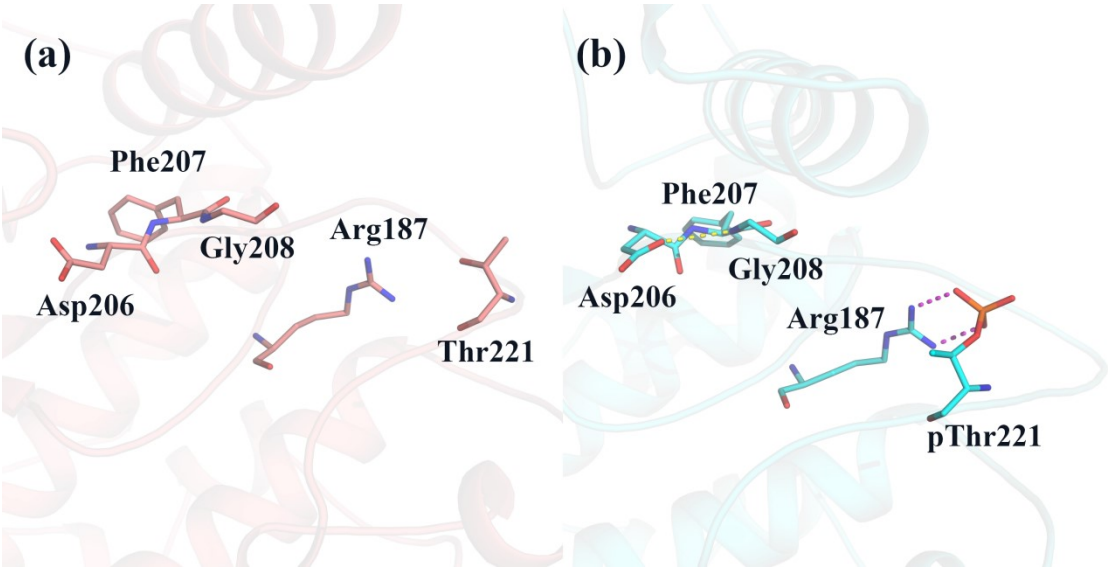

Figure S2. Impact of T221 phosphorylation on key interactions within conserved kinase motifs. (a) WT SIK3. (b) SIK3-pT221. Left panels: backbone hydrogen bonds within the DFG motif (Asp206–Gly208). Right panels: a salt bridge between Arg187 of the HRD motif and pT221, which appears exclusively in the phosphorylated state.

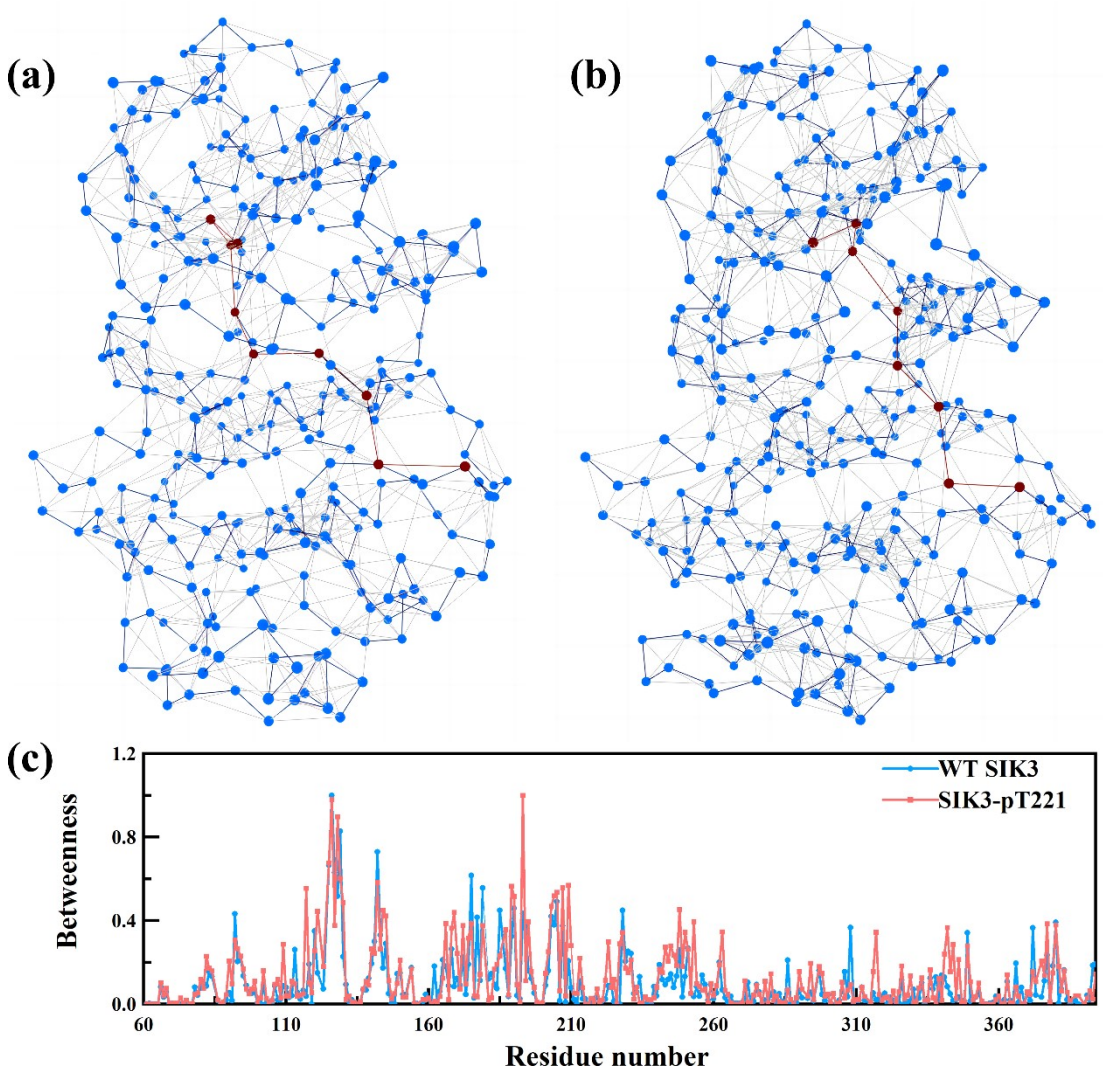

Figure S3. Network analysis of allosteric communication pathways in SIK3. (a) The shortest communication path between the β3 strand (Lys95) and T221 in the WT SIK3 network. (b) The shortest path between β3 (Lys95) and pT221 in the phosphorylated SIK3 network. (c) Betweenness centrality of each residue in the WT versus phosphorylated networks, showing enhanced centrality in key regions upon phosphorylation. The WT SIK3 system is shown in blue, and the SIK3-pT221 system is shown in light red.

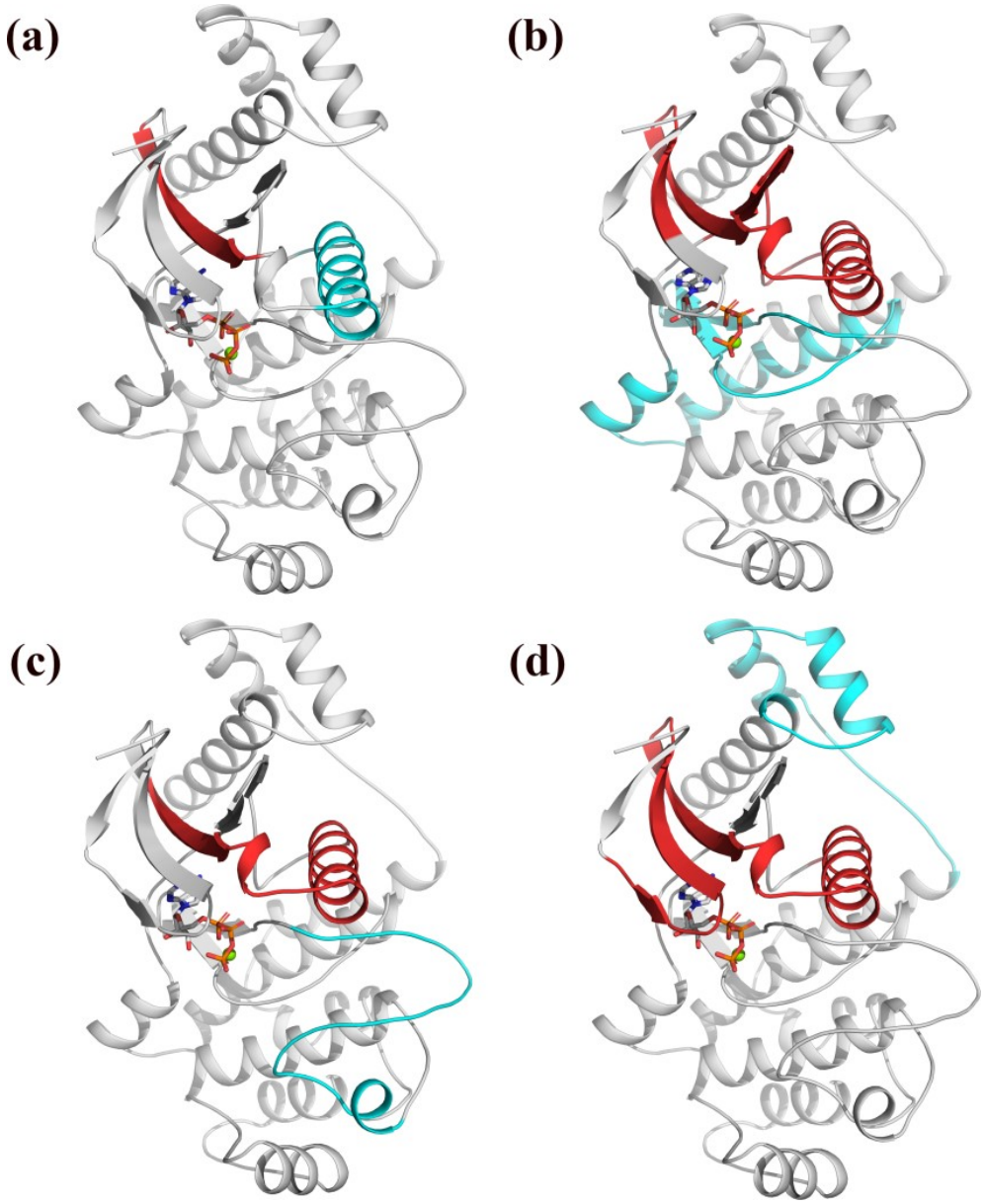

Figure S4. Structural mapping of correlation hotspots (R1–R4) identified in the DCCM analysis. Structural illustrations highlight the following regions: (a) Region R1 – encompassing the αC-helix and β3-sheet. (b) Region R2 – the interface between the C-lobe and N-lobe. (c) Region R3 – comprising the A-loop, αC-helix, and β3-sheet. (d) Region R4 – spanning the N-lobe and the UBA domain. The structural regions corresponding to the x- and y-axes in Figures 5a and 5b are highlighted in cyan and red, respectively.

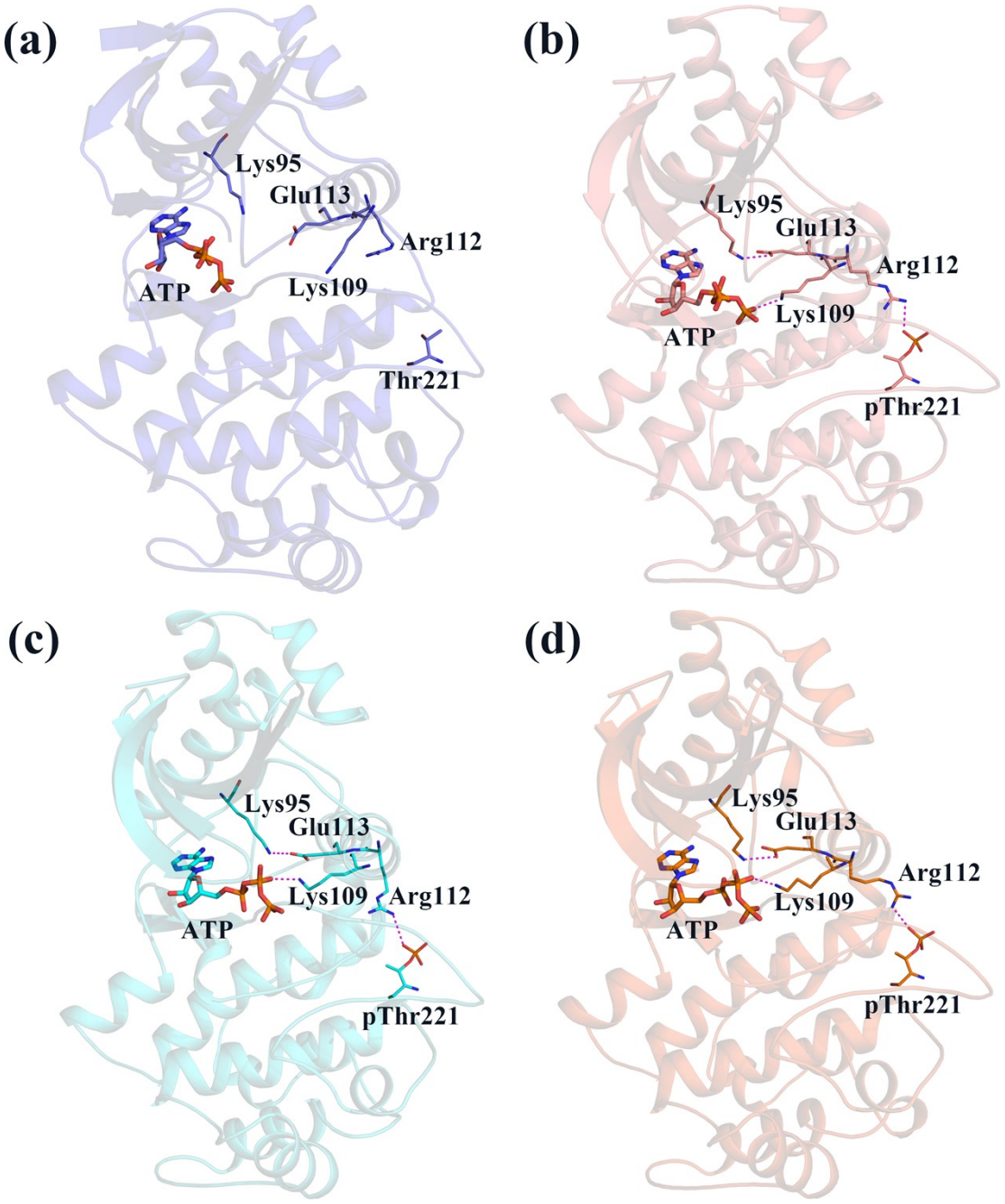

Figure S5. Representative structures from the major free-energy basins and associated salt-bridge interactions. (a) Representative structure of the dominant basin in WT SIK3. (b–d) Representative structures of the three lowest-energy basins in SIK3-pT221. Protein is shown as cartoon, while key residues and ATP are shown as sticks. Purple dashed lines indicate key salt-bridge interactions.

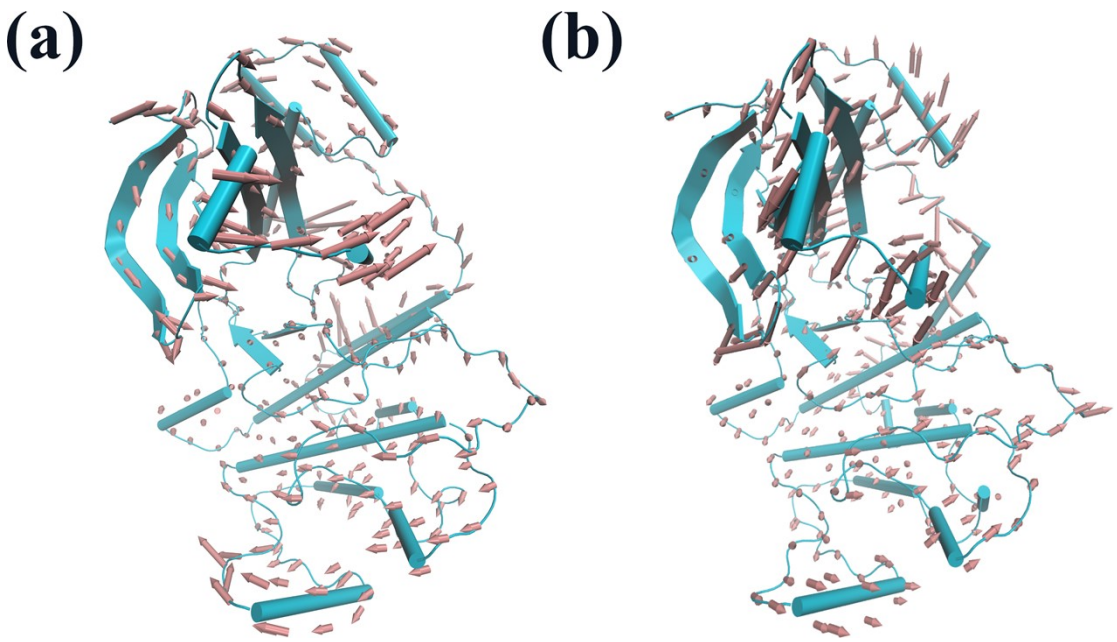

Figure S6. Dominant motion modes of SIK3 revealed by principal component analysis. Pink arrows (eigenvectors) represent the predominant motion directions of backbone Cα atoms in the WT SIK3 and SIK3-pT221 systems. Arrow length reflects the relative magnitude of each motion mode.